


ORIGINAL ARTICLE

Open Access



Fretting Wear Characteristics of Nuclear Fuel Cladding in High-Temperature Pressurized Water

Jun Wang¹, Haojie Li¹, Zhengyang Li², Yujie Lei¹, Quanyao Ren², Yongjun Jiao² and Zhenbing Cai^{1*} 

Abstract

In pressurized water reactor (PWR), fretting wear is one of the main causes of fuel assembly failure. Moreover, the operation condition of cladding is complex and harsh. A unique fretting damage test equipment was developed and tested to simulate the fretting damage evolution process of cladding in the PWR environment. It can simulate the fretting wear experiment of PWR under different temperatures (maximum temperature is 350 °C), displacement amplitude, vibration frequency, and normal force. The fretting wear behavior of Zr-4 alloy under different temperature environments was tested. In addition, the evolution of wear scar morphology, profile, and wear volume was studied using an optical microscope (OM), scanning electron microscopy (SEM), and a 3D white light interferometer. Results show that higher water temperature evidently decreased the cladding wear volume, the wear mechanism of Zr-4 cladding changed from abrasive wear to adhesive wear and the formation of an oxide layer on the wear scar reduced the wear volume and maximum wear depth.

Keywords Fretting wear, Cladding, High temperature and high pressure, Zirconium alloy

1 Introduction

After more than 70 years of development, the main type of nuclear reactor in the world is the pressurized water reactor (PWR) [1]. The fuel rod, one of the core components of the nuclear power reactor, operates in bad conditions, including irradiation, flow-induced vibration, and high-temperature high pressure (HTHP). In the reactor, water is used as the cooling and heat transfer medium, and the high-speed fluid flowing from bottom to top and around the fuel assembly in the reactor core will induce the irregular vibration of the cladding, which is called fluid-induced vibration [2–4]. As the service time of the

cladding increases, the clamping force of the grid to the cladding is relaxed, and under the effect of flow-induced vibration, the fuel rod vibrates with hundreds of microns amplitude, resulting in grid-to-rod fretting (GTRF) [2, 3]. The survey report shows that the flow-induced vibration is the main reason for the failure and fracture of the cladding [1–3]. Therefore, studying the fretting wear of fuel rods during the service process of PWR systematically is necessary. In addition, corresponding experimental equipment is required to carry out relevant scientific research. For example, Ming et al. [5] designed and manufactured a load distribution measuring instrument to measure the friction force during the operation of the cam mechanism. Duranty et al. [6] fabricated a linear reciprocating tribometer to study the wear behavior of polymers in a high-pressure hydrogen environment.

A corresponding experimental device should be developed to simulate the fretting wear of the fuel rods during the operation of the PWR as much as possible. Kim et al. [7] used a sliding wear tester and a sliding

*Correspondence:

Zhenbing Cai
czb-jiaoda@126.com

¹ Key Lab of Advanced Technologies of Materials, Tribology Research Institute, Southwest Jiaotong University, Chengdu 610031, China

² Science and Technology on Reactor System Design Technology Laboratory, Nuclear Power Institute of China, Chengdu 610213, China



© The Author(s) 2023. **Open Access** This article is licensed under a Creative Commons Attribution 4.0 International License, which permits use, sharing, adaptation, distribution and reproduction in any medium or format, as long as you give appropriate credit to the original author(s) and the source, provide a link to the Creative Commons licence, and indicate if changes were made. The images or other third party material in this article are included in the article's Creative Commons licence, unless indicated otherwise in a credit line to the material. If material is not included in the article's Creative Commons licence and your intended use is not permitted by statutory regulation or exceeds the permitted use, you will need to obtain permission directly from the copyright holder. To view a copy of this licence, visit <http://creativecommons.org/licenses/by/4.0/>.

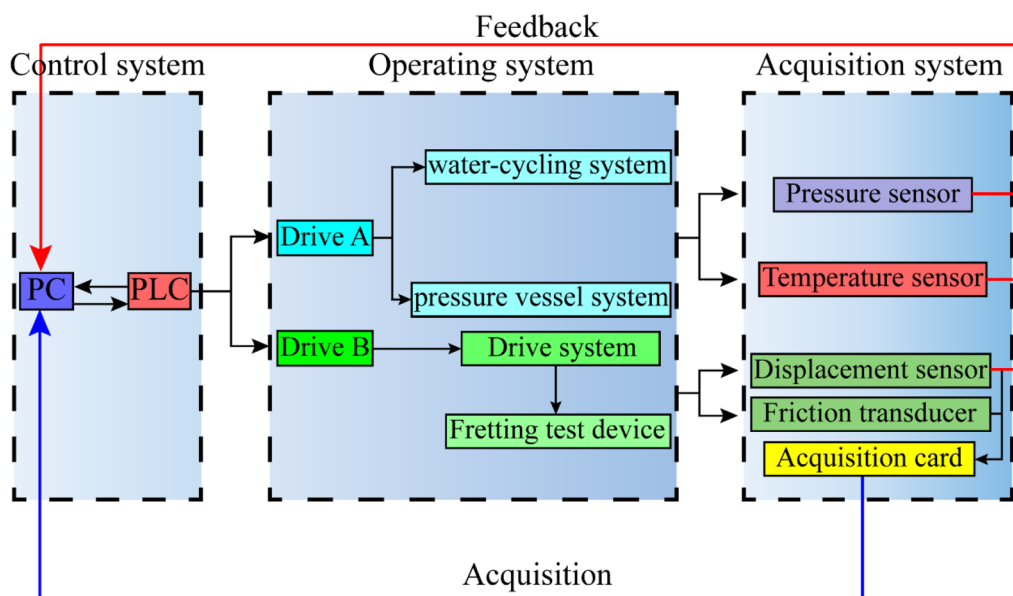


Figure 1 Block diagram of the control system

impact wear tester to study the influence of various contact forms on the fretting wear of cladding tubes at room temperature. The result showed that the contact shape affected the fretting state evidently. Lee et al. [8] developed an impact/sliding wear tester to study the influence of impact frequency on the impact wear of spring support tubes under 300 °C water. Park et al. [9] investigated the wear behavior of Zr alloy tubes under different water temperatures (20 °C, 50 °C, and 80 °C) by using unique fretting wear equipment. They found that as the water temperature increased, the surface microhardness decreased. Besides, the wear depth and area decreased with the increase in viscosity. Qu et al. [2] designed a tester to study the influence of pre-oxidation on the wear coefficient of Zr alloy cladding at room temperature. Then, Lazarevic et al. [3, 10] investigated the fretting wear of the Zr alloy tubes at 204 °C temperature pressurized water environment by developing a unique autoclave fretting rig. In addition, Guo et al. [11–14] designed and manufactured a tangential fretting abrasion testing machine for simulating the experimental environment of a pressurized water reactor. The effect of different wear parameters and surface modification treatment on the fretting abrasion of zirconium alloy cladding and 690 alloy [15–18] was studied. The maximum test conditions were 320 °C.

However, thus far, most of these studies were conducted in air or water at temperatures well below 320 °C. The data and conclusions of the previous works [19–22] provide substantial information not only to understand the fretting behavior of the heat transfer tubes and fuel

rods but also to design a nuclear power plant. However, the data are still insufficient. Moreover, the influence mechanism of various fretting parameters on the fretting damage of cladding is unclear. In this study, fretting wear test equipment for simulating the experimental environment of a pressurized water reactor with a maximum operating temperature of 350 °C and 20 MPa was designed and manufactured. The fretting damage behavior of the fuel rod under the operating conditions of the primary circuit of PWR was investigated.

2 Design Details of HTHP Fretting Test Rig

2.1 Block Diagram of the Control System

Figure 1 is the block diagram of the control system of the unique instrument. The measuring system consists of a control system, an operating system, and an acquisition system. The PC inputs the edited control program into PLC. Then, the PLC sends instruction A to control the operation of the booster pump and heat exchanger to improve the pressure and temperature of the water environment and instruction B to control the linear driver to drive the linear motor movement. The signals of friction and displacement from the friction transducer and displacement sensor are collected by the NI acquisition card. A feedback signal including the pressure and temperature of the water environment and displacement of the linear motor is analyzed by the PC to decide whether to send out a new control signal. The signals of pressure and temperature of the water environment are collected by a pressure sensor and temperature sensor.

Table 1 Functional parameters of the instrument developed

Item	Parameter
Temperature (°C)	0–350
Pressure (MPa)	0–20
Normal load (N)	20–60
Displacement (μm)	10–1000
Frequency (Hz)	1–15

The functional parameters of the instrument are listed in Table 1. The temperature, pressure, displacement, and normal load can be adjusted in any way desired.

2.2 Structural Detail

Figure 2 shows the structural detail of the instrument. The device consists of five modules, which are called: pressure vessel system (A), fretting test device (B), water circulation system (C), drive system (D), and control system. The fretting device is installed inside the autoclave,

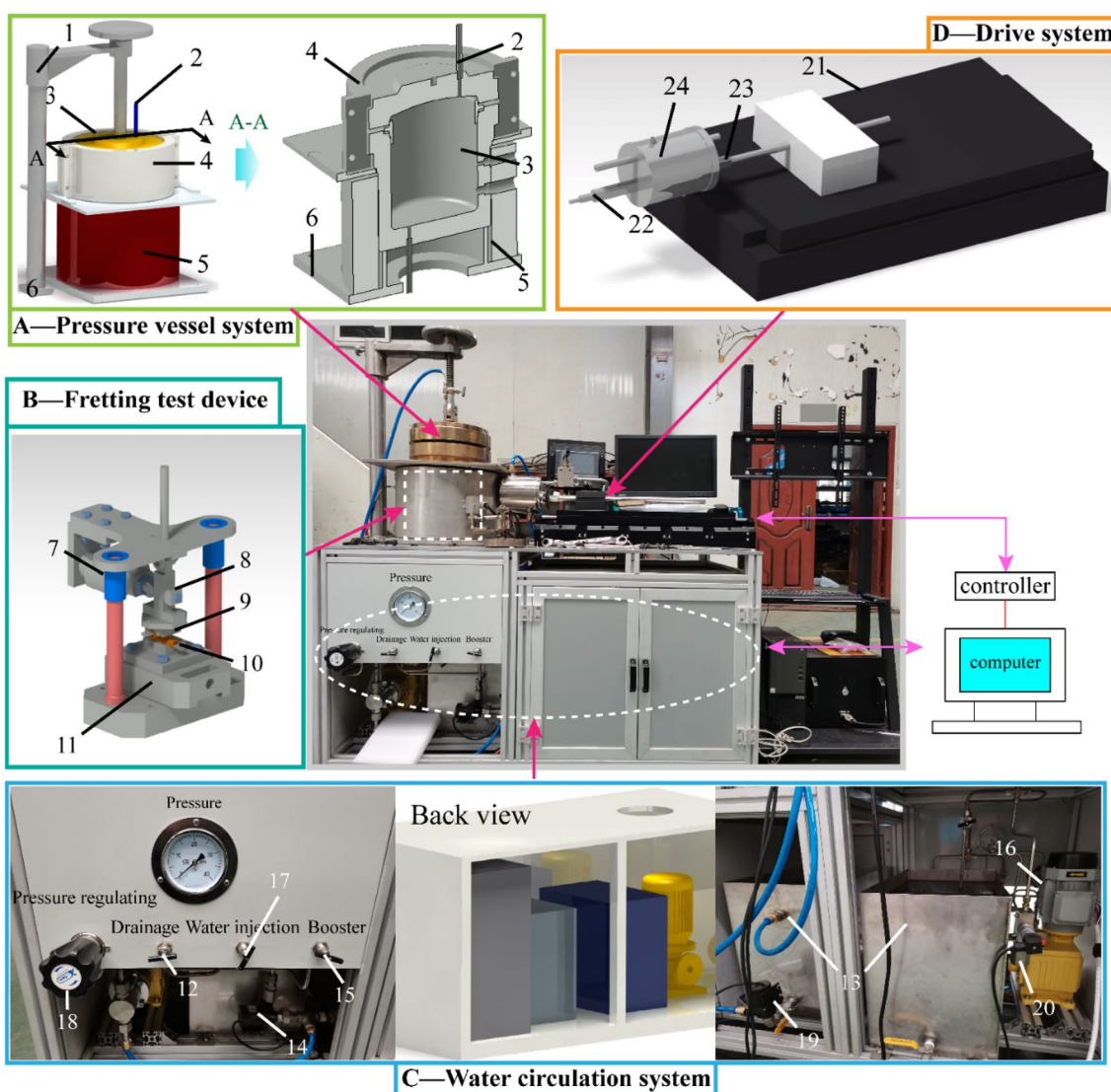


Figure 2 Structural detail of the HTHP fretting test rig: 1-lifting mechanism, 2-exhaust valve, 3-autoclave, 4-locking clamp, 5-ceramic heater, 6-support seat, 7-force sensor, 8-swing rod, 9-friction pair, 10-tube sample, 11- sliding block, 12- drainage valve, 13- water tank, 14- water pump a, 15- booster valve, 16- booster pump, 17- water injection valve, 18- pressure regulating valve, 19- water pump b, 20- back pressure valve, 21- linear motor, 22- transmission shaft, 23-sealing ring, 24- cooling reflux device

and the maximum design pressure of the whole device is 22 MPa and the design temperature is 350 °C.

The pressure vessel system is composed of a lifting mechanism (1), an exhaust valve (2), an autoclave (3), a locking clamp (4), a ceramic heater (5), and a support seat (6), presenting the basics of the whole device. An autoclave is placed under the lifting mechanism used to open and close the autoclave cover. At the beginning of the test, water is injected into the autoclave through the feed water pump 1. Then, the booster pump is turned on to increase the pressure of the autoclave until a specified pressure. Finally, the exhaust valve on the autoclave is turned off, and the ceramic heater is used to increase the temperature of the autoclave to the rated temperature. The pressure and temperature signals of the water environment are collected by the pressure and temperature sensors, respectively. A feedback signal including water pressure and temperature is transmitted to the computer during the test. After computer analysis, the water environment temperature and pressure are adjusted to ensure that the experiment is carried out under the specified pressure and temperature.

As shown in Figure 2, the fretting test device consists of two parts. The upper part is equipped with a force sensor (7), swing rod (8), friction pair (9), and weights. Then, the lower part is equipped with a tube sample (10) and sliding block (11). The friction pair is fixed on the fixture assembled on the swing rod, and the sample is mounted on the fixture of the sliding block. The preload (normal load " P ") is applied by different deadweight loading. A transmission shaft with a water jacket passes through the autoclave wall and connects the sliding block with the linear motor to provide a driving force to move the sliding block. A friction transducer, which is fixed on the oscillating bar, collects the friction data between the sample and the friction pair during the fretting wear experiment and transmits them to the computer.

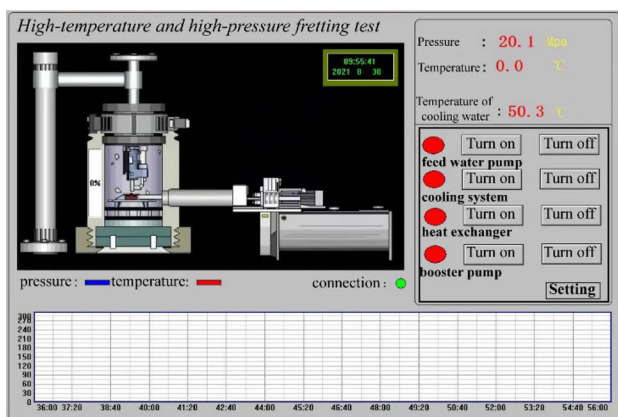
The water circulation system is the core part of the instrument, which is the circulating water supply system of the whole equipment. The drainage valve (12) must be closed before the test. The water in the water tank (13) is added to the autoclave through the feed water pump *a* (14). Then, the booster valve (15) is opened to continuously inject water into the autoclave through the booster pump (16). Close the water injection valve (17) after emptying the air in the autoclave. The control program automatically adjusts the switch of the pressure regulating valve (18) according to the temperature and pressure feedback signal from the sensors to adjust the temperature and pressure in the autoclave when the autoclave heats up. At the same time, another water pump *b* (19) began to provide cooling water for the cooling reflux device and collect the used water.

To prevent accidents, a back pressure valve (20) for emergency pressure relief is equipped to prevent damage to the kettle body caused by excessive pressure in the autoclave. Pressure and temperature indicators are used to monitor the pressure and temperature in the autoclave in real-time.

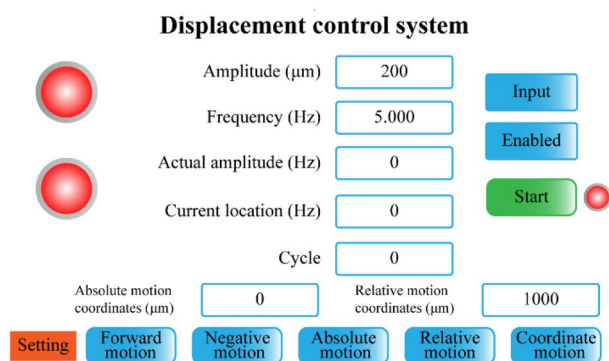
The drive system, which consists of a linear motor (21), a transmission shaft (22), sealing rings (23), and a cooling reflux device (24), is another core component of the instrument. The linear motor and wear test device are connected through a transmission shaft with a cooling reflux device. Achieving the dynamic seal of the device is important because the experimental environment is an HTHP water environment, it also involves fretting. Then, two sealing rings were used inside the water jacket to prevent the leakage of HTHP water in the autoclave and circulating water inside the water jacket. Generally, the service temperature of the commercial sealing ring is lower than 300 °C. Therefore, circulating cooling water must be continuously introduced into the cooling reflux device to reduce the temperature at the sealing ring. The sealing ring is closely connected with the transmission shaft and the sealing port to maintain the sealing performance given the small vibration amplitude during the test. At the same time, the cooling water reduces the temperature at the sealing ring to ensure that it can be used for a long time. In this way, the dynamic sealing of the equipment is effectively completed.

2.3 Control and Acquisition System

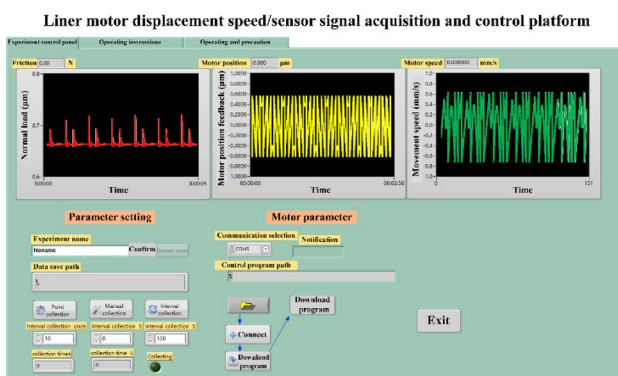
Figures 3(a, b) show the control interfaces of the pressure vessel system and drive system, respectively. The self-made control program A (Figure 3(a)) is downloaded from the PC to the controller to control the operation of the booster pump and heat exchanger to improve the pressure and temperature of the water environment. Another program B (Figure 3(b)) controls the linear driver to drive the linear motor movement. The feedback signal including pressure and temperature of the water environment is analyzed by the PC to determine whether to continue heating or maintain this temperature. Meanwhile, the signal of the displacement is very important for the acquisition system. The signal acquisition system is developed based on the LabVIEW, the displacement was measured by the grating ruler and processed by the encoder throughout the test. The parameters related to the sensor are as follows: the measurement range is ± 445 N, the temperature range is -54 °C to 121 °C, the temperature coefficient of sensitivity is ≤ 0.09 %/°C, sensitivity ($\pm 15\%$) is 11241 mV/kN. The measurement accuracy of the micro grating system is 0.5 μm . The instrument is developed to carry out fretting wear experiments under the HTHP water environment. The constraint of the



(a) Control interface of the pressure vessel system



(b) Control interface of the drive system



(c) Control interface of the acquisition system

Figure 3 Interface of the control and acquisition system of the instrument

sample's shape and size is determined by the user. If a different sample test is required, then the shape and size of the clamp should be changed.

3 Experiment

The traditional commercial Zr-4 cladding and domestic substitute material N36 zirconium alloy used in PWR is selected as the research objects. The size of Zr-4 cladding: length = 15 mm, external diameter = 10 mm, and wall thickness = 0.73 mm. The size of the N36 tube is as follows: length = 15 mm, external diameter = 9.5 mm, and inner diameter = 8.36 mm. The composition of N36 and Zr-4 is shown in Table 2.

Based on the vibration simulation by Westinghouse Electric Company and Oak Ridge National Laboratory [2, 3, 10, 23] and the data provided by the Nuclear Power Institute of China (NPIC), the normal load, displacement amplitude, and frequency were selected as 20 N, 100 μm, and 5 Hz, respectively. The inlet temperature of the reactor is about 290 °C, and the outlet temperature is about 315 °C. Therefore, the following four temperatures are selected for the experiment (RT, 90 °C, 260 °C, and 315 °C) to investigate the effect of different temperatures on the fretting abrasion of the cladding. The test parameters are listed in Table 3. The test duration was 3 hours. First, the sample and friction pair were assembled on the fretting test device, and the pressure vessel system was closed. Second, water was injected into the autoclave through the water injection valve, and the exhaust valve, drainage valve, and pressure regulating valve were closed. Third, the heating device was turned on, and the exhaust valve was opened to discharge the oxygen in the autoclave when the temperature was up to 140 °C and the pressure was 0.2 MPa. Finally, the linear motor controlled by the PC was turned on when the temperature reached the specified value. All tests were repeated three times. The wear area and volume are average values, and there are error bars.

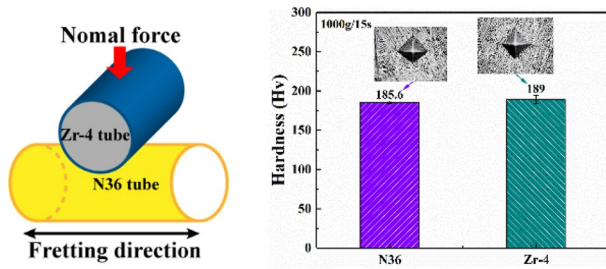
Before the fretting wear test, the hardness was tested. The load and hold time are 1000 g and 15 s, respectively. The hardness of the Zr-4 cladding and N36 are 185.6±2.1 HV and 189±1.4 HV, respectively. Figure 4 shows the sample assembly diagram and the hardness of the two materials. The specimens were immersed in ethanol and cleaned by ultrasonication. After the test, the samples were examined

Table 2 Composition of samples (wt%)

Chemical composition	Nb	Sn	Fe	Cr	O	Zr
Zr-4	–	1.7	0.24	0.13	0.14	Bal.
N36	1.07	0.95	0.33	–	0.13	Bal.

Table 3 Parameters for fretting wear test

Testing parameters	Value
Temperature (°C)	RT, 90 °C, 260 °C, 315 °C
Normal load (N)	20
Displacement (μm)	100
Frequency (Hz)	5
Cycles	5×10 ⁴



(a) The assembly diagram (b) Hardness
Figure 4 Assembly diagram and hardness of samples

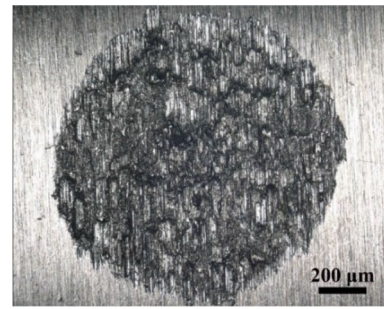
using an optical microscope (OM), scanning electron microscopy (SEM), and 3D white light interferometer.

4 Results and Discussion

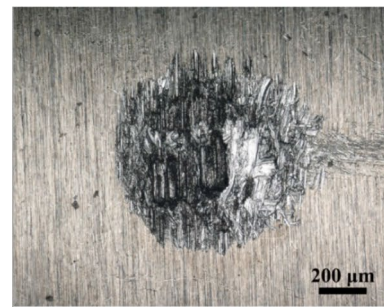
4.1 Morphologies of Worn Surfaces

The morphologies of the worn surface of Zr-4 cladding are presented in Figure 5. The area of the worn surface initially decreases and then increases with the increase in temperature. When the temperature is higher than 90 °C, the surface color of the cladding changes; it is different from the samples at 90 °C and RT. As shown in Figure 5(c, d), the oxide layer is formed on the surface, and a ring named friction influence area (between the yellow and red dotted line) that is distinguishable from the worn area and the unworn area appears around the wear scar. The area of the wear scar on the cladding under RT water was larger than that in higher temperature (at 260 °C and 315 °C) water, indicating that the damage in low-temperature may be more severe than in high-temperature water.

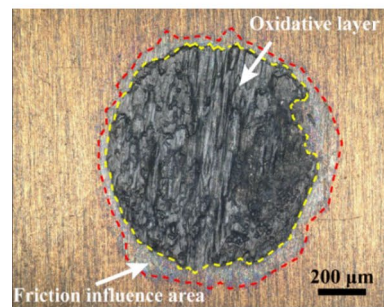
Figure 6 is the 3D morphology of the wear scar of the Zr-4 cladding under various temperatures. The 3D microscopic image shows that the overall wear scar is shallow, and some deep pits in the worn surface. Besides, the width of the wear scar decreases from 1206 μm to 856 μm with the temperature increase. The wear scar characteristics of the samples tested below 260 °C (Figure 6(a, b)) show different morphologies from those of 315 °C



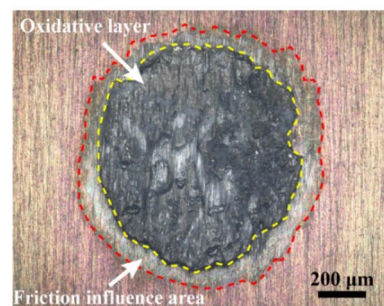
(a) RT



(b) T=90 °C



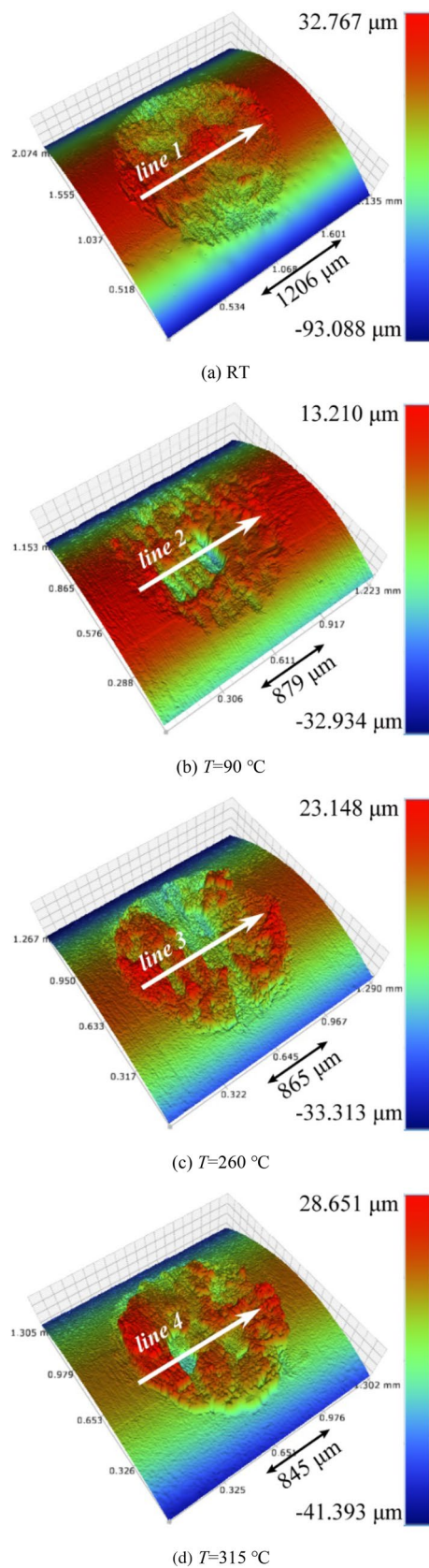
(c) T=260 °C



(d) T=315 °C

Figure 5 OM images of the wear scar of Zr-4 claddings under different temperatures

(Figure 6(c, d)). Under 260 °C, grooves are found in the whole worn surface in the same direction as the vibration, and the distribution of grooves is relatively random. At 315 °C (Figure 6(d)), debris accumulation layers



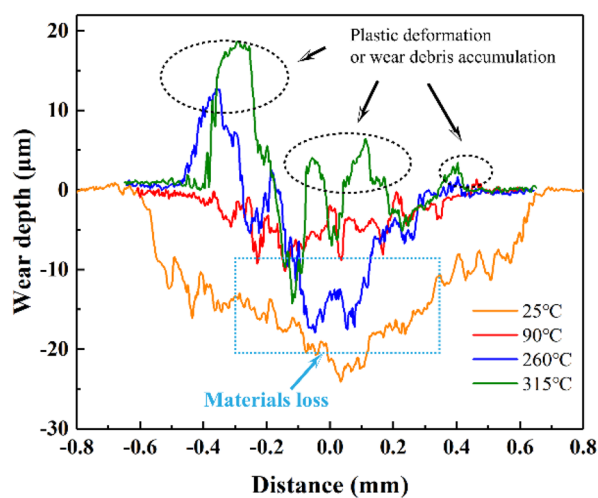
◀ **Figure 6** 3D morphology of the wear scar of the Zr-4 claddings under various temperatures

are evident, the worn surface is raised, and the furrow becomes larger and deeper.

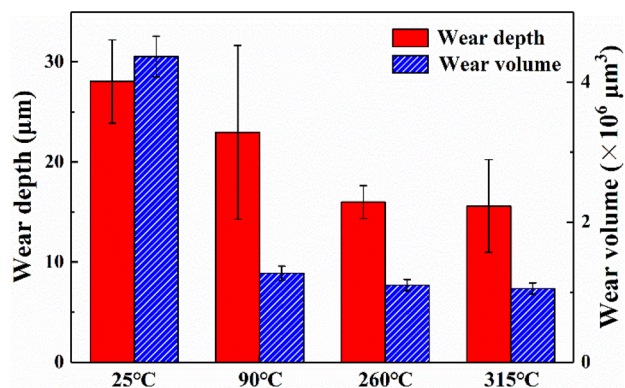
Figure 7(a) shows the profiles of Zr-4 claddings (lines 1 to 4 in Figures 6 (a–d)). From the profiles, the overall profile is a “U” profile below 315 $^{\circ}\text{C}$, indicating that the main wear mechanism is abrasive wear. However, in the environment of 260 $^{\circ}\text{C}$ and 315 $^{\circ}\text{C}$, many bumps appear on the worn surface. This is due to the wear debris being squeezed and sintered during the fretting process, eventually forming a dense wear debris accumulation layer on the worn surface. It shows that the material softens and the wear mechanism changes to adhesive wear as the temperature increases.

The wear depth and volume of the Zr-4 claddings are presented in Figure 7(b). The average wear depth and wear volume decrease when the temperature increases. At RT and 90 $^{\circ}\text{C}$, the wear mechanism of Zr-4 cladding is still abrasive wear. However, as the temperature increases from RT to 90 $^{\circ}\text{C}$, the contact area increases due to metal expansion and the maximum contact stress decreases [16], so that the wear volume decrease. The wear debris mainly composed of ZrO_2 [24] condenses together and forms large wear grains. The relatively hard wear grains trace a series of randomly distributed furrows on the contact surface, causing some worn surfaces with serious damage in the middle and others with serious damage at the edge [25], thus leading to a large dispersion of wear depth at 90 $^{\circ}\text{C}$. According to the results of 3D morphologies and profiles of wear scar, the fretting wear mechanism gradually changes to adhesive wear as the temperature increases further, at this time, the friction pair material was transferred, and a wear debris accumulation layer was formed on the worn surface, which plays an important role in antifriction and lubrication thus reducing the wear volume of Zr-4 claddings.

Figure 8 shows the SEM image and element composition of the wear scar of claddings. As shown in Figures 8(a, b), the O element was mainly concentrated in the worn surface under the lower temperature while it (Figure 8(c, d)) is evenly distributed in the wear area and the without wear area under the higher temperature. The oxidation phenomenon on the surface of the sample is gradually obvious as the temperature increases. Meanwhile, the morphological characteristics of the worn surface change with temperature. At RT (Figure 8(a)) and 90 $^{\circ}\text{C}$ (Figure 8(b)), the characteristics of the worn surface were mainly furrowed and delamination, but when the temperature rose to 260 $^{\circ}\text{C}$ (Figure 8(c)) and 315 $^{\circ}\text{C}$



(a) Wear scar profiles



(b) Wear depth and volume

Figure 7 Wear scar profiles, depth, and volume of Zr-4 tubes

(Figure 8(d)), the worn surface shows typical adhesive wear characteristics such as bonding.

Figure 9 presents an enlarged view of the worn surface (in the white wireframe of Figure 8). Much loose wear debris and oxides accumulated in the wear scar area below 260 °C, accompanied by many furrows and delamination, as shown in Figures 9(a, b). Moreover, the surface was rough, indicating that the wear mechanism was delamination and abrasive wear. However, the wear scar gradually became smooth and flat, the delamination phenomenon was not evident, and the surface furrow was evident when the temperature ascended to 315 °C (Figure 9(d)). Besides, an oxidized layer in which the surface is smooth on a macroscopic scale, as shown in Figure 9(d), namely the “glaze layer” [26] has been formed on the worn surface, indicating that the main wear mechanism was adhesion wear and abrasive wear.

The chemical composition at the typical positions of wear scar is listed in Table 4. The date of EDS showed

a higher O: Zr ratio at a higher temperature, indicating that the surface oxidation degree increases. The element composition of the two materials (Table 2) shows that Nb is a unique element of N36 alloy. No evident Nb element was detected by EDS analysis below 260 °C (sites A–F), whereas the content of the Nb element in the formed oxide film increased more than 10 times at 315 °C (sites G and H). This is due to the softer cladding and grid materials when the temperature increases, causing more significant adhesive wear and abrasive wear [3], and material transfer occur to the friction pair.

4.2 Cross-sectional Analysis

To further analyze the influence of temperature on the fretting wear mechanism of Zr-4 cladding, the cross-section morphology of the wear scar under various temperatures was examined, as shown in Figures 10 and 11. The sectional morphology of the Zr-4 cladding at RT is shown in Figure 10. Figure 10(a) is the overall morphology of the wear scar. The magnified image as shown in Figures 10(b, c) shows many furrows and micro-cracks in the edge of the wear scar, which is the typical abrasive wear and delamination morphology. The EDS results show no obvious oxide layer formation on the surface of the furrows and wear scar, which further confirms that the wear mechanism under this state is mainly abrasive wear. The SEM morphology of the central area of the wear scar (Figure 10(d)) and EDS mapping can see that oxygen elements are concentrated on the worn surface, indicating that part of the wear debris is oxidized during the wear process, while no obvious oxide layer is produced on the cross-section. Figure 10(e) is the section magnified morphology in the white wireframe of Figure 10(d). The debris accumulation layer which is attached to the worn surface is loose, full of holes, and stratified. Proved that fretting wear under RT condition is mainly abrasive wear and delamination.

Figure 11 shows the sectional morphology of the Zr-4 cladding at 315 °C. As shown in Figure 11(a), the width of the wear scar decreases with the increase in temperature. The SEM images and EDS mapping of the center area of the wear scar in Figure 11(b) have shown that a layer of the white dense oxide layer is produced on the worn surface, which is significantly different from the wear debris accumulation layer at room temperature. EDS line results (Figure 11(f)) show that the oxide layer thickness in the central area of the wear scar is about 15 μm. As shown in Figure 11(c) and Figure 11(d) (that is the section magnified morphology in the white wireframe of Figure 11(c)), a large number of cobweb-like cracks were observed at the edge of the wear scar. From the EDS line

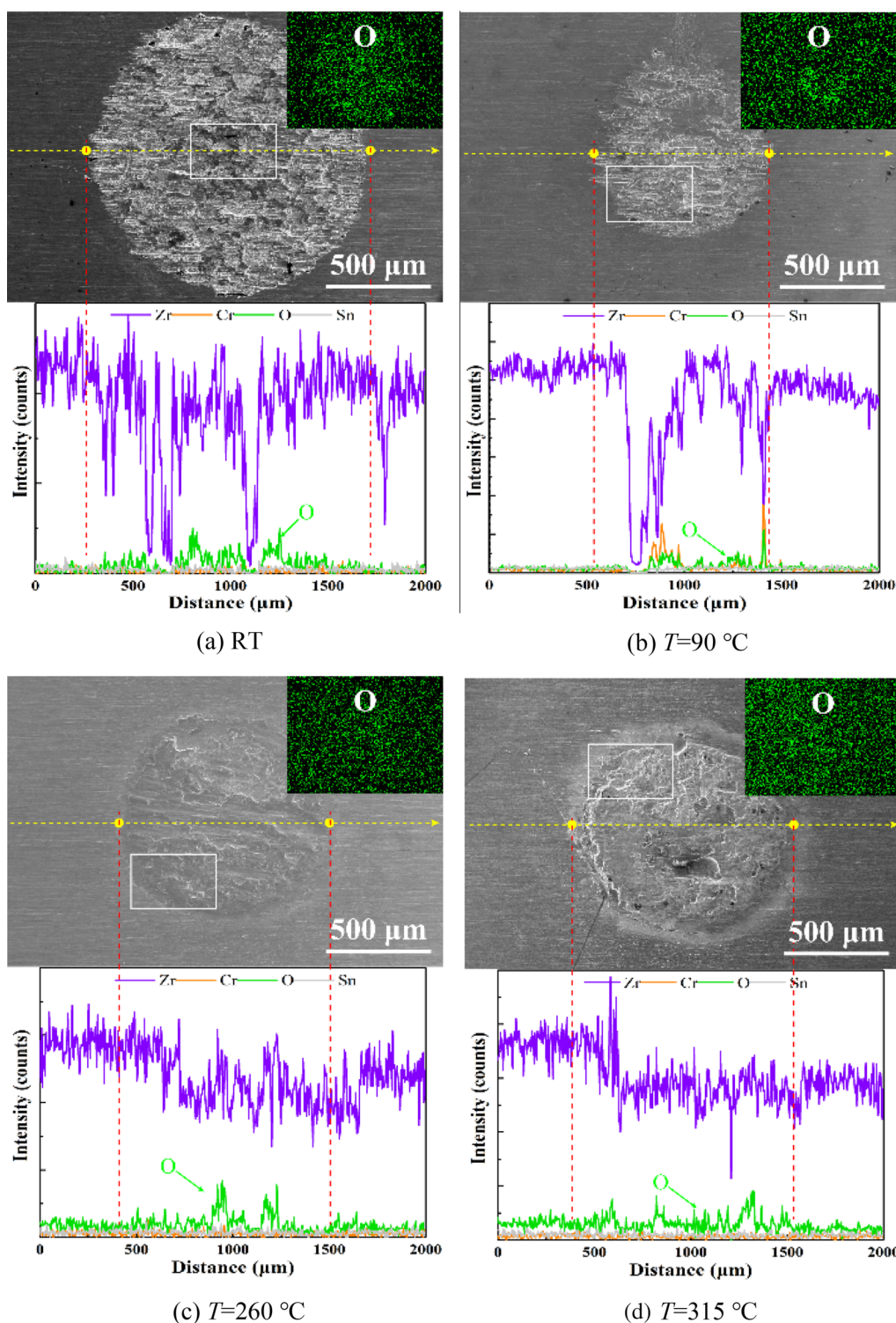


Figure 8 SEM morphologies of wear scar under different temperatures

scanning results (Figure 11(e)), it can be observed that the thickness of the oxide layer in this area is about 8 μm . The oxygen content in the area full of cracks fluctuates

sharply and is slightly higher than that of the matrix. This area is the friction influence layer between the oxide layer and the matrix.

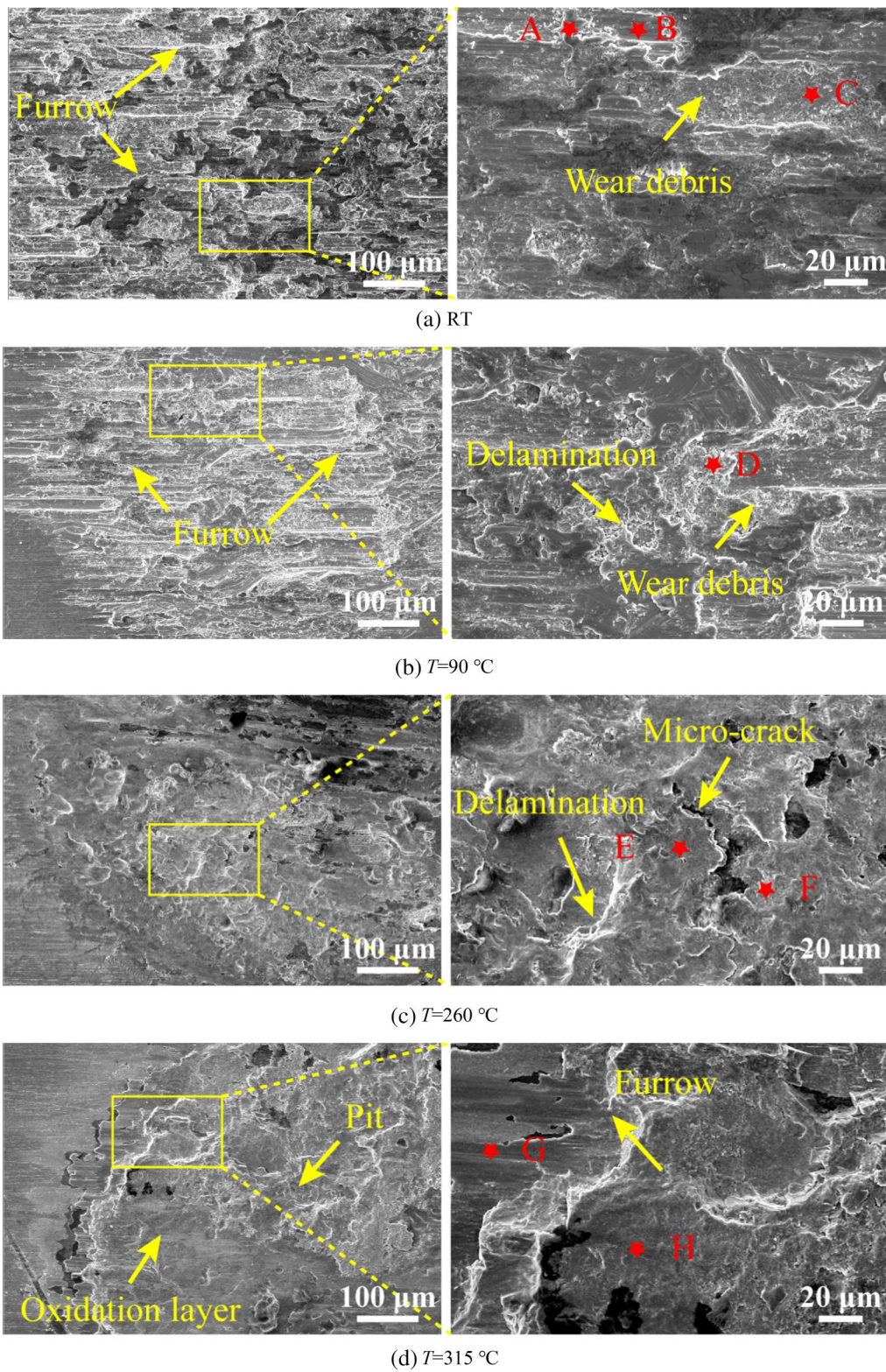
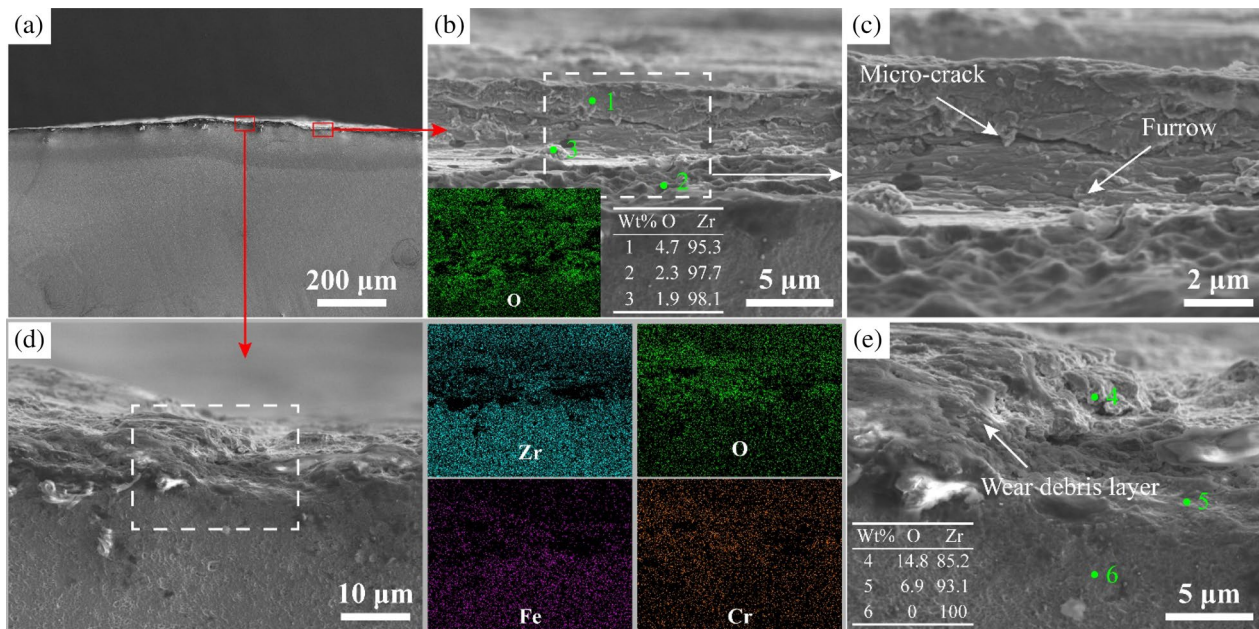


Figure 9 SEM images of the center micro area of the white wireframe in Figure 8

Table 4 EDS results of site A-J in Figure 9 (wt%)

Element	B	C	D	E	F	G	H
O	2.89	9.20	10.41	6.96	11.85	11.39	14.07
Fe	0.09	0.22	0.39	0.28	0.26	0.28	0.39
Zr	94.66	88.63	86.63	79.19	77.31	80.37	76.24
Nb	1.08	0.85	1.48	12.93	9.75	6.82	8.79
Sn	1.28	1.11	1.09	0.65	0.84	1.14	0.52

**Figure 10** Cross-sectional images of the wear scar (RT)

4.3 Discussion

The above results, including optical microscope morphology, 3D morphology, wear scar profile, SEM morphology, and EDS composition, indicate that the fretting wear behavior is vitally affected by the environmental temperature. The 3D topography and wear scar profile were observed, and the results showed that material transfer occurred in the higher temperature environment, the material transfer was further confirmed by cross-sectional features and EDS analysis of the surface elements of the wear scar. The wear mechanism has changed from abrasive wear and delamination to adhesive wear.

With the increase in temperature, the cladding and friction pair become softer and the shear strength decreases [27–29], and the viscosity of water decreases as the temperature rises; the lubricating effect decreases, resulting in more evident abrasive wear and adhesive wear and the transfer of friction pair materials and accumulation on the relatively hard surface of the cladding [12, 30–32]. Under the action of cyclic contact stress, contact fatigue occurs on the contact area,

which induces the generation of micro-cracks and rapidly expands around. The wear debris accumulates on the contact surface and undergoes compression and sintering in the presence of high temperature and high pressure (HTHP) water, resulting in the formation of a thick and compact oxide layer known as the "glaze layer" [26]. This glaze layer tightly adheres to the worn surface, effectively protecting the clad tube from further wear, reducing frictional losses, providing lubrication, and ensuring cladding integrity. [22, 33–35]. The "glaze layer" in the central area of the worn surface is thick, while the edge area is thin. This is because the contact area between the sample and the pair, that is, the central area of the wear scar, is an adhesive area. The crack initiation at the edge of the wear scar is caused by contact fatigue during fretting, which tears the material in the adhesive area from the pair and adheres to the sample. Finally, a thick "glaze layer" is formed under the action of HTHP water. The formation of a glaze layer can protect the cladding, thus reducing the wear volume of the cladding.

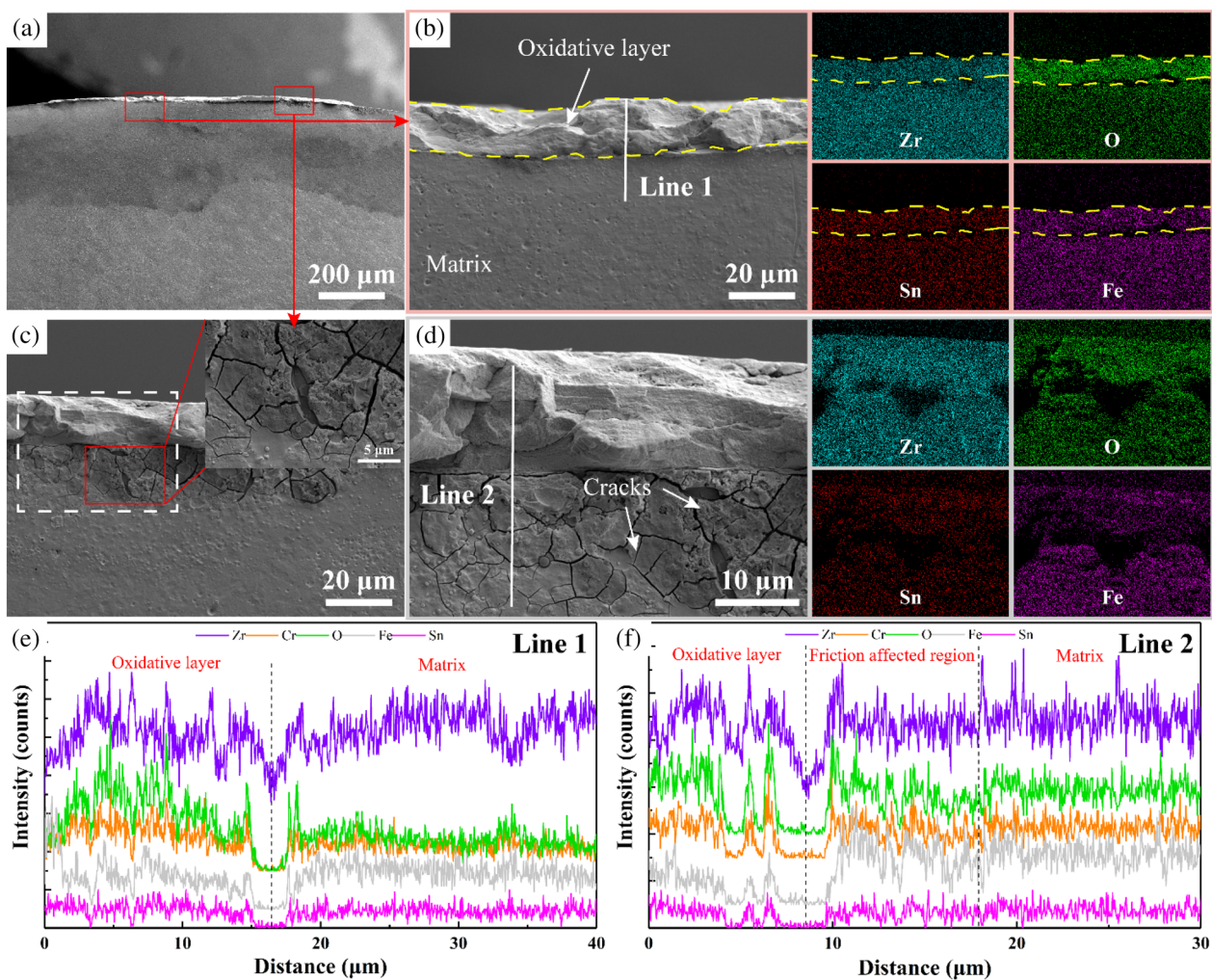


Figure 11 Cross-sectional images of the wear scar ($T=315\text{ }^{\circ}\text{C}$)

5 Conclusions

A fretting wear test rig simulating the working condition of PWR was designed and manufactured. The wear test of Zr-4 cladding under different temperatures was investigated. The main conclusions are as follows.

- (1) The wear volume and depth of Zr-4 cladding decreased rapidly with a higher water temperature. The wear volume of cladding in $315\text{ }^{\circ}\text{C}$ pressurized water was reduced by 75% compared to the RT environment.
- (2) Temperature is a key factor leading to changes in the wear mechanism of Zr-4 cladding. The main wear mechanism of Zr-4 cladding changed from abrasive wear and delamination to adhesive wear when the temperature increased from RT to $315\text{ }^{\circ}\text{C}$.
- (3) As the temperature increases, severe adhesive wear can lead to contact fatigue in the contact area, lead-

ing to wear debris accumulation on the surface of the Zr-4 cladding. Under the action of HTHP, wear debris forms a glaze layer on the worn surface that has the function of reducing wear and lubrication.

Acknowledgements

Not applicable.

Author Contributions

JW and YL were in charge of the whole trial; JW wrote the manuscript; JW, ZC, and YJ assisted with sampling and laboratory analyses. HL, ZL, and QR assisted in components design and manufacture. All authors read and approved the final manuscript.

Author's Information

Jun Wang, born in 1991, is a PhD candidate at Southwest Jiaotong University, China. His main research interest is fretting wear.

Haojie Li, born in 1997, is a master candidate at Southwest Jiaotong University, China. His main research interest is fretting wear.

Zhengyang Li, born in 1992, is currently an engineer at the Nuclear Power Institute of China, China. His main research interests include fuel element design and manufacturing.

Yujie Lei, born in 1997, is a master candidate at Southwest Jiaotong University, China. His main research interest is fretting wear.

Quanyao Ren, born in 1991, is currently an engineer at the Nuclear Power Institute of China, China. His main research interests include nuclear power plant reactor structure design.

Yongjun Jiao, born in 1971, is currently the chief designer at the key science and technology project of CNNC's fuel element design and manufacturing technology, and the chief designer at the Nuclear Power Institute of China, China.

Zhenbing Cai is currently a professor and a PhD supervisor at Southwest Jiaotong University, China. His main research interests include tribology, surface engineering, and the service behavior of key parts of large equipment (high-speed railway, nuclear power, etc.)

Funding

Supported by National Key R&D Program of China (Grant No. 2022YFB3401901), Key Program of National Natural Science Foundation of China (Grant No. U2067221), Sichuan Provincial Science and Technology Planning Project (Grant Nos. 2022JDJQ0019 and 2022ZYD0029), Funds for China Postdoctoral Science Foundation (Grant No. 2022M713008) and Sichuan Provincial Innovative Talent Funding Project for Postdoctoral Fellows (Grant No. BX202225).

Availability of Data and Materials

The datasets supporting the conclusions of this article are included within the article.

Declarations

Competing Interests

The authors declare no competing financial interests.

Received: 14 November 2022 Revised: 28 July 2023 Accepted: 1 August 2023

Published online: 04 September 2023

References

- [1] Z Cai, Z Li, M Yin, et al. A review of fretting study on nuclear power equipment. *Tribology International*, 2020, 144: 106095.
- [2] J Qu, KM Cooley, AH Shaw, et al. Assessment of wear coefficients of nuclear zirconium claddings without and with pre-oxidation. *Wear*, 2016, 356-357: 17-22.
- [3] S Lazarevic, RY Lu, C Favade, et al. Investigating grid-to-rod fretting wear of nuclear fuel claddings using a unique autoclave fretting rig. *Wear*, 2018, 412-413: 30-37.
- [4] CET M J Pettigrew, N J Fisher, M Yetisir, et al. Flow-induced vibration: recent findings and open questions. *Nuclear Engineering and Design*, 1998, 185: 249-276.
- [5] SL Ming, JF Wang, ZB Cai, et al. Load distribution measurement instrument for oscillating follower cam mechanism. *Review of Scientific Instruments*, 2019, 90: 045114.
- [6] ER Duranty, TJ Roosendaal, SG Pitman, et al. An in situ tribometer for measuring friction and wear of polymers in a high pressure hydrogen environment. *Review of Scientific Instruments*, 2017, 88: 095114.
- [7] H-K Kim, Y-H Lee. Influence of contact shape and supporting condition on tube fretting wear. *Wear*, 2003, 255: 1183-1197.
- [8] Y-H Lee, H-K Kim, Y-H Jung. Effect of impact frequency on the wear behavior of spring-supported tubes in room and high temperature distilled water. *Wear*, 2005, 259: 329-336.
- [9] YC Park, SH Jeong, YH Kim, et al. Influence of temperature on the fretting wear of advanced nuclear fuel cladding tube against supporting grid. *Key Engineering Materials*, 2007, 345-346: 705-708.
- [10] C Kumara, R Wang, RY Lu, et al. Grid-to-rod fretting wear study of SiC/SiC composite accident-tolerant fuel claddings using an autoclave fretting bench test. *Wear*, 2022, 488-489: 204172.
- [11] X Guo, P Lai, L Tang, et al. Effects of sliding amplitude and normal load on the fretting wear behavior of alloy 690 tube exposed to high temperature water. *Tribology International*, 2017, 116: 155-163.
- [12] L Zhang, P Lai, Q Liu, et al. Fretting wear behavior of zirconium alloy in B-Li water at 300 °C. *Journal of Nuclear Materials*, 2018, 499: 401-409.
- [13] P Lai, H Zhang, L Zhang, et al. Effect of micro-arc oxidation on fretting wear behavior of zirconium alloy exposed to high temperature water. *Wear*, 2019, 424-425: 53-61.
- [14] P Lai, J Lu, H Zhang, et al. The corrosion behavior of M5 (Zr-1Nb-0.120) alloy in 360 °C water with dissolved oxygen. *Journal of Nuclear Materials*, 2020, 532: 152079.
- [15] H Ming, X Liu, Z Zhang, et al. Effect of normal force on the fretting wear behavior of Inconel 690 TT against 304 stainless steel in simulated secondary water of pressurized water reactor. *Tribology International*, 2018, 126: 133-143.
- [16] X-C Liu, H-L Ming, Z-M Zhang, et al. Effects of temperature on fretting corrosion between alloy 690TT and 405 stainless steel in pure water. *Acta Metall Sin (Engl)*, 2019, 32: 1437-1448.
- [17] H Ming, X Liu, J Lai, et al. Fretting wear between alloy 690 and 405 stainless steel in high temperature pressurized water with different normal force and displacement. *Journal of Nuclear Materials*, 2020, 529: 151930.
- [18] Y Zhang, H Ming, L Tang, et al. Effect of the frequency on fretting corrosion behavior between Alloy 690TT tube and 405 stainless steel plate in high temperature pressurized water. *Tribology International*, 2021, 164: 107229.
- [19] Z-b Cai, X-d Chen, T Rui, et al. Investigation of the fretting corrosion mechanism of QPQ-treated TP316H steel in liquid sodium at 450 °C. *Corrosion Science*, 2022, 201: 110282.
- [20] X-d Chen, S Feng, L-w Wang, et al. Effect of QPQ on the fretting wear behavior of TP316H steel at varying temperatures in liquid sodium. *Journal of Nuclear Materials*, 2022, 562: 153583.
- [21] Y-q Yu, X-d Chen, L-y Yang, et al. Investigation on fretting wear behavior of 2.25Cr-1Mo tube in water at various temperatures. *Wear*, 2021, 476: 203727.
- [22] T Yu, G Fu, Y Yu, et al. Wear characteristics of the nuclear control rod drive mechanism (CRDM) movable latch serviced in high temperature water. *Chinese Journal of Mechanical Engineering*, 2022, 35: 26.
- [23] H Jiang, J Qu, RY Lu, et al. Grid-to-rod flow-induced impact study for PWR fuel in reactor. *Progress in Nuclear Energy*, 2016, 91: 355-361.
- [24] MH Attia, A de Pannemaecker, G Williams. Effect of temperature on tribo-oxide formation and the fretting wear and friction behavior of zirconium and nickel-based alloys. *Wear*, 2021, 476: 203722.
- [25] Z Zhang, S Pan, N Yin, et al. Multiscale analysis of friction behavior at fretting interfaces. *Friction*, 2020, 9: 119-131.
- [26] P Lai, X Gao, L Tang, et al. Effect of temperature on fretting wear behavior and mechanism of alloy 690 in water. *Nuclear Engineering and Design*, 2018, 327: 51-60.
- [27] A Gilat, XR Wu. Plastic deformation of 1020 steel over a wide range of strain rates and temperatures. *International Journal of Plasticity*, 1997, 13: 611-632.
- [28] AM Iskandarov, SV Dmitriev, Y Umeno. Temperature effect on ideal shear strength of Al and Cu. *Physical Review B*, 2011, 84: 224118.
- [29] R Khazaka, L Mendizabal, D Henry. Review on joint shear strength of nano-silver paste and its long-term high temperature reliability. *Journal of Electronic Materials*, 2014, 43: 2459-2466.
- [30] AIT Kayaba. Effect of the hardness of hardened steel and the action of oxides on fretting wear. *Wear*, 1981, 66: 27-41.
- [31] GH M. Varenberg, I. Etsion. Different aspects of the role of wear debris in fretting wear. *Wear*, 2002, 252: 902-910.
- [32] K Elleuch, S Fouvry. Experimental and modelling aspects of abrasive wear of a A357 aluminium alloy under gross slip fretting conditions. *Wear*, 2005, 258: 40-49.
- [33] S Zhou, Y Shen, H Zhang, et al. Heat treatment effect on microstructure, hardness and wear resistance of Cr26 white cast iron. *Chinese Journal of Mechanical Engineering*, 2015, 28(1): 140-147.
- [34] Z-B Cai, J-F Peng, H Qian, et al. Impact fretting wear behavior of Alloy 690 tubes in dry and deionized water conditions. *Chinese Journal of Mechanical Engineering*, 2017, 30(4): 819-828.
- [35] T Chen, L Song, S Li, et al. Experimental study on wear characteristics of pcbn tool with variable chamfered edge. *Chinese Journal of Mechanical Engineering*, 2019, 32: 37.